JCTC Journal of Chemical Theory and Computation

A Multiscale Treatment of Angeli's Salt Decomposition

Juan Torras,[†] Gustavo de M. Seabra,[‡] and Adrian E. Roitberg[‡]

Departament d'Enginyeria Química, EUETII, Universitat Politècnica de Catalunya, Pça. Rei 15, 08700-Igualada, Spain, and Quantum Theory Project, Departments of Physics and of Chemistry, University of Florida, Gainesville, Florida 32611-8435

Received June 20, 2008

Abstract: Sodium trioxodinitrate's ($Na_2N_2O_3$, Angeli's salt) unique cardiovascular effects have been associated with its ability to yield HNO upon dissociation under physiological conditions. Due to its potential applications in new therapies for heart failure, the dissociation of Angeli's salt has recently received increased attention. The decomposition mechanism has been previously studied by quantum mechanical methods using a continuum approximation (PCM) for the solvent effects. In this work we use our recently developed interface of the Amber and Gaussian packages via the PUPIL package to study Angeli's salt dissociation in a hybrid QM/MM scheme where the water solvent molecules are treated explicitly with classical mechanics while the solute is treated with full quantum mechanics (UB3LYP/6−31+G(d) and UMP2/6−31+G(d)) level. Multiple steered molecular dynamics was used with the Jarzynski relationship to extract the free energy profile for the process. We obtain 4.8 kcal mol^{-1} and 6.4 kcal mol^{-1} free energy barriers for the N−N bond breaking for UB3LYP and UMP2, respectively. The geometries and Mulliken charges for reactant, transition state, and products have been characterized through a number of hybrid QM/MM molecular dynamics runs with the N−N distance restrained to representative values of each species. The results highlight the role of individual solvent molecules for the reaction energetics and provide a comparison point against implicit solvation methods.

Introduction

In aqueous solution and in biological media, Angeli's salt, $Na_2N_2O_3$ (AS, compound **1**, Scheme 1),[3,4] spontaneously decomposes to yield the critical bioregulatory species nitroxyl (HNO/NO^-) and has been widely used in studies of nitroxyl's pharmacological properties.[3−10] Similarities in structures and decomposition rates of Angeli's salt and NO donors such as diethylamine-NO ($Na[Et_2NN(O)NO]$, DEA/NO) have allowed comparison between the properties of NO and HNO, revealing that, although some of pharmacological HNO properties are similar to that of NO,[5,6] the cardiovascular effects elicited by HNO are often distinct.[7,8]

The suggested mechanism for the decomposition of Angeli's salt at physiological pH is believed to involve the protonation of the dianion $N_2O_3^{2-}$ on the NO oxygen to form **(2)**, followed by tautomerization into **(3)** and heterolytic cleavage of the N−N bond releasing HNO **(4)** and NO_2^- **(5)**, as depicted in Scheme 1 [the numbering in (**3**) shows the convention adopted here].

The dissociation of Angeli's salt in anaerobic medium was recently the subject of a thorough quantum mechanical study at the B3LYP/6−311+G(d) level of theory by Houk et al.,[1] where the aqueous solvation energies were estimated by single point calculations with implicit water, represented by the Polarizable Continuum Model (PCM),[9−12] on the vacuum-optimized B3LYP/6−311+G(d) structures and applied to the gas-phase energies. Some key structures were also reoptimized with PCM and the same basis set. The results of that breakthrough work support the mechanism depicted in Scheme 1 at physiological pH. The free energy barrier for the N−N bond cleavage step was computed as 6.0 kcal/mol in vacuum, changing to 7.8 kcal/mol when the structures are reoptimized with PCM.[1] A later experimental and theoretical study of AS decomposition in aerobic conditions concluded

* Corresponding author e-mail: roitberg@ufl.edu.
[†] Universitat Politècnica de Catalunya.
[‡] University of Florida.

10.1021/ct800236d CCC: $40.75
Published on Web 12/12/2008

Scheme 1. Proposed Mechanism for Angeli's Salt Decomposition Pathway in Anaerobic Media

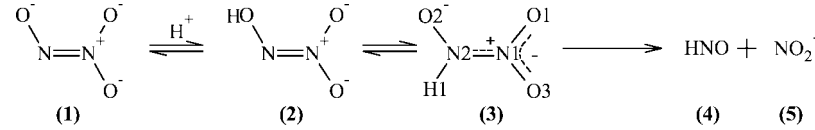

that interaction with O_2 is likely to occur only after the N−N bond breakage.[7]

In the previous work, the free energies were obtained by performing a standard vibrational frequency and thermochemistry analysis, which yields the thermal energy corrections to enthalpies and free energies. Thermochemical quantities are calculated from the partition function using the equations for noninteracting particles (ideal gas) in the canonical ensemble, such as described in statistical thermodynamics textbooks.[13] The solvent effects were included by using the Polarizable Continuum solvent Model (PCM) which has the advantage of greatly reducing the size of the system by approximating the bulk solvent by a homogeneous dielectric continuum polarizable by the solute, which is placed in a molecular-shaped cavity.[9−12] The computational speedup however comes at the price of neglecting the atomistic nature of the solvent, and the solvent configurational sampling is assumed to be implicit, ignoring local anisotropies around the solute. The basic assumption of continuum models is the notion that the implicit part of the system (solvent) is well described by the bulk dielectric constant. This also assumes that the structure and dynamics of individual solvent molecules can be neglected. This assumption obviously fails for the first solvation shells and especially in the case of ionic compounds. Evidently the choice of the system to be treated as the solute is then critical, and recent studies indicate that, in some cases, inclusion of explicit solvent molecules treated at the same level of theory as the solute of interest may be required.[14,15]

Other alternatives for the inclusion of solvent effects that explicitly take into consideration the structure of the solvent include the use of molecular mechanics (MM) methods for configurational sampling, followed by full QM calculations on snapshots taken from the MM trajectories, with the solvent molecules included as point charges. An example of this strategy are the MD/QM[16,17] and MC/QM[18−22] methods which use classical force fields and Molecular Dynamics (MD) or Monte Carlo (MC) for configurational sampling, respectively. Implicit in those methods, however, is the assumption of reasonable overlap between the conformational space sampled by the QM and MM potential energy surfaces.

Another possibility, which is the method of choice in the present study, is the use of hybrid QM/MM simulations, where a sampling method such as MD[23,24] or MC[25,26] is used as before, but the energy is calculated by dividing the system into two parts: a small section containing the portion of interest (solute) and treated by quantum mechanics, plus the remainder of the system (e.g., solvent) treated using classical force fields. The MD or MC equations are then propagated on this hybrid QM/MM surface.

Since a QM calculation is required at every MD or MC step, most implementations of QM/MM use semiempirical quantum Hamiltonians, such as the native QM/MM support present in the latest version of the MD program AMBER (Amber 9).[27−29] (With the exception of fully quantum methods such as Car−Parrinello[30] or Born−Oppenheimer Molecular Dynamics,[31,32] the complexity of those methods, however, limits the size of the system that can be accurately treated.) These semiempirical methods have the shortcoming of yielding unpredictable results if the system differs significantly from the molecules present in the parametrization set. For more unusual molecules a full QM method may be necessary, and interfaces have been designed between MM and QM programs for that purpose, such as ChemShell,[33] QoMMMa,[34] and, more recently our own, the PUPIL package,[2,35] developed initially in the Materials Science field for the integration of arbitrary molecular dynamics and quantum mechanics programs.[36,37]

We have recently reported[2] interfaces of the PUPIL package with the widely used programs Gaussian[38] (for quantum mechanics) and Amber[27,39] (Molecular Dynamics). The advantage of the PUPIL implementation lies in the fact that the software packages communicate directly and exclusively with the PUPIL interface: Whenever forces are needed for the QM atoms during the MD calculation, AMBER requests those from PUPIL, which then uses the QM program of choice (Gaussian03 in the present case) to calculate those forces and communicate them back to AMBER. Since each package is an independent unit, it is possible to use any method available in either package.

In the present work we report the application of the Gaussian/PUPIL/Amber interface for the study of the Angeli's salt dissociation (Scheme 1) in explicit water, avoiding the shortcomings of implicit solvation models. The N-protonated Angeli's salt (**3**) is treated quantum mechanically and immersed in a box of classical TIP3P[40] water molecules. The Free Energy Profile for the N−N bond cleavage is calculated by Multiple Steering Molecular Dynamics,[41,42] which is implemented in AMBER. The present results are compared to previous calculations[1] to show the relevance of explicit consideration of solvent molecules.

Theory

QM/MM. In the hybrid QM/MM scheme[23,24] used here the system is partitioned in two regions: a quantum mechanical (QM) region comprising a small number of atoms relevant to the specific problem being treated and a classical mechanics (MM) region with all the remaining atoms. The final Hamiltonian for such system can be written as

$$\hat{H} = \hat{H}^{QM} + \hat{H}^{MM} + \hat{H}^{QM/MM} \quad (1)$$

where $\hat{H}^{QM}$ is the Hamiltonian for the QM part, calculated using the QM program and method of choice, and $\hat{H}^{MM}$ is the Hamiltonian for the MM part, calculated by the MM program using the usual force field equations. The remaining

term, $\hat{H}^{QM/MM}$, describes the interaction between the QM and MM parts and typically contains terms for electrostatic, van der Waals, and bonded interactions across the region boundaries:

$$\hat{H}^{QM/MM} = \hat{H}^{QM/MM}_{vdW} + \hat{H}^{QM/MM}_{elect} + \hat{H}^{QM/MM}_{bonded} \quad (2)$$

In PUPIL's QM/MM implementation, the $\hat{H}^{QM/MM}_{vdW}$ term is calculated as usual by the MM program, using the standard 12−6 Lennard-Jones in eq 3, and parameters derived from the force field in use for both the QM and MM atoms. It has been shown that the use of the MM parameters in this interaction does not introduce significant errors in the calculation.[43]

$$E^{QM/MM}_{vdW} = \sum_{\alpha}^{QM}\sum_{A}^{MM}\left[\frac{A_{\alpha A}}{R^{12}_{\alpha A}} - \frac{B_{\alpha A}}{R^{6}_{\alpha A}}\right] \quad (3)$$

The electrostatic interaction between the QM and MM regions can be divided in two parts. First, the influence of the MM atoms on the QM zone is taken into account by electronic embedding: The MM atoms are passed to the QM program as point charges fixed at their respective positions, using the charge values from the force field parameters. Second, the force contribution from the quantum atoms to the total force acting upon each classical atom (F^{QM}_i) is needed. Gaussian03 uses a fast multipole method to evaluate the effect of the external charges onto the QM system, allowing for a very fast calculation. However, this formalism does not allow us to compute the forces from the QM region onto the MM charges. In the present implementation these forces are obtained after the QM calculation by projecting the obtained electronic density into a grid (a Gaussian Cube file) and calculating the interaction of the MM charge with each point in the grid as in

$$F^{QM}_i = \sum_{j}^{N_{cube}} \mathbf{r_{ij}} \frac{q_{PC_i} dq_j}{|r_{ij}|^3} \quad (4)$$

where q_{PC_i} is the MM point charge, N_{cube} is the total number of electron density points, and

$$dq_j = \rho_j dx dy dz \quad (5)$$

defines an individual volume element on the electron density grid.

If covalent bonds cross the boundaries of the QM/MM system PUPIL can use a link atom approach,[44] where a new quantum particle (link atom) is introduced along the bond between the QM and MM region at a specific distance, usually around 1 Å, in order to satisfy valence requirements. The approach used by PUPIL has been described in more detail elsewhere.[2]

Free Energies via Multiple Steering Molecular Dynamics. The accurate calculation of the free-energy change along the chemical reaction path remains a challenge, and different methods have been developed to deal with this issue.[24,42,45−68] The multiple steering molecular dynamics (MSMD) method relates a system's nonequilibrium dynamics to its equilibrium properties and has been described in more detail elsewhere,[41,42,59,69−72] so only a short summary is presented here.

Consider a system subject to an external time-dependent perturbation [$\lambda=\lambda(t)$] and described by the Hamiltonian $H(\mathbf{r},\lambda)$. Writing $\Delta G(\lambda)$ as the free energy change and $W(\lambda)$ as the external work performed on the system as it evolves from an initial to a final state ($\lambda_0 \rightarrow \lambda$), the free energy and work are connected by the Jarzynski relationship[42]

$$e^{-\beta\Delta G(\lambda)} = \langle e^{-\beta W(\lambda)} \rangle \quad (6)$$

where the brackets represent an average taken over an ensemble of molecular dynamics trajectories starting at different snapshots extracted from an equilibrated ensemble at the initial distance. It is important to note that eq 6 assumes a converged average, which is formally true only with an infinite number of process realizations. In practical applications standard deviations up to a few kT are considered acceptable (see, for example, ref 61), and the error in ΔG can be estimated by

$$\Delta G \approx \langle W \rangle - \frac{\beta}{2}\sigma^2_W \quad (7)$$

which is just the result of a cumulant expansion of eq 6[42] and is the same as the fluctuation−dissipation relation obtained earlier by Hermans.[73]

Also, the equilibrium average of a state function can similarly be extracted from the nonequilibrium ensemble by[69,70]

$$\langle F(\lambda) \rangle_{eq} = \frac{\langle F(\lambda) e^{-\beta W(\lambda)} \rangle_{non-eq}}{\langle e^{-\beta W(\lambda)} \rangle_{non-eq}} \quad (8)$$

The time-dependent Hamiltonian $H(\mathbf{r},\lambda)$ can be written as the sum of the time-independent Hamiltonian for the unperturbed system, $H_0(\mathbf{r})$, and a time-dependent external perturbation, which here is chosen as a harmonic potential whose minimum moves at a constant velocity, v. Representing the chosen reaction path as $\lambda(\mathbf{r})$, one can write

$$H(\mathbf{r},\lambda) = H_0(\mathbf{r}) + \frac{1}{2}k[\lambda(\mathbf{r}) - \lambda_0 - vt]^2 \quad (9)$$

The free energy of a process along the chosen reaction coordinate can then be calculated by performing a large number of simulations, each being one independent realization of the process and starting from a different snapshot extracted from an ensemble initially equilibrated at $\lambda=\lambda_0$ and then properly averaging the resulting work values as described in eq 6.

Computational Methods. Due to the computational demands of the QM methods applied here, a scheme was devised to avoid long equilibrations at the QM level, which involved the equilibration of the system in a sequence of steps of increasing complexity. According to this scheme, the system was first equilibrated and brought to 300 K by fully classical molecular dynamics and then relaxed at the approximated density functional SCC-DFTB[74] level. Finally, the initial structures chosen for the pulling simulations were further relaxed at the final UB3LYP/6−311G(d,p)and UMP2/6−311G(d,p) levels.

Parameters for the Angeli's Salt. Even though the Angeli's salt is to be treated quantum mechanically classical parameters are still needed since in the PUPIL system the

MD program has no knowledge of the quantum system and the parameter arrays still need to be correctly filled, and also because classical MD simulations are performed in the initial relaxation. Those parameters are not used for the final analysis, where the solute is treated with full quantum mechanics.

Starting from the published coordinates from Dutton et al.[1] (a07, supplemental information), the Antechamber[27] program was used in conjunction with DIVCON[75−77] to generate General Amber Force Field (GAFF)[78] parameters for the Angeli's salt, using AM1-BCC[79,80] charges. All those programs are part of the standard Amber distribution.[27]

System Preparation. The system was comprised of one molecule of the N-protonated Angeli's salt **(3)**, one Na^+ ion added to neutralize the system, and a total of 2388 water molecules (TIP3P),[40] under periodic boundary conditions. This system was first subjected to 10,000 minimization steps, using the MM Hamiltonian to remove any clashes, and then heated to 300 K during 100 ps at constant volume. A time step of 1.0 fs and using a Langevin thermostat with a 2.0 ps^{-1} collision frequency were used. Finally, the system was allowed to relax for an additional 100 ps at constant pressure (1 atm) with a pressure relaxation time of 1 ps, still using a fully MM Hamiltonian. All of these steps used the SHAKE algorithm to restrain bonds containing hydrogen.[81] Next, the solute (**3**) was made quantum, to be treated with the approximated Self-Consistent-Charge Density-Functional Tight-Binding SCC-DFTB method,[74,82] which we recently implemented in the Amber package,[28] and the remainder of the system (water molecules plus Na^+ ion) was treated classically. The system was then relaxed again (using Amber's native QM/MM implementation[28,29]) for another 50 ps with constant volume, then 500 ps constant pressure, and the same parameters as for the fully classical steps. At this point, the system was considered to be sufficiently equilibrated, and another 2 ns run at constant volume was used to extract the average N−N distance, r_{eq} (1.29 Å).

Generation of an Equilibrated Initial Ensemble (Forward Reaction). The Jarzynski equality assumes that all pulling processes start from structures belonging to the same initial equilibrated ensemble. To generate the initial structures, the N−N distance was restrained to a number slightly smaller than r_{eq} by applying a harmonic potential centered at 1.27 Å with a large force constant (2500 kcal mol^{-1} $Å^{-2}$) and run a 3 ns QM/MM simulation using the SCC-DFTB Hamiltonian for the solute, extracting 20 structures from the last 2 ns. Finally, we run another 1000 steps of MD using the Amber/PUPIL/Gaussian interface to treat the Angeli's salt as quantum at a much more computationally expensive level, the unrestricted form of Becke's 3-parameter hybrid functional[83] (UB3LYP) with the 6−311+G(d)[84,85] basis set, as implemented in Gaussian, while the rest of the system is treated by MM, so that the starting structures are consistent with this level of theory.

Multiple Steered Molecular Dynamics (MSMD). Forward Reaction. With the structures properly equilibrated at the initial distance, the N−N bond in each structure was broken using the Amber/PUPIL/Gaussian interface by running independent simulations starting from each of the 20 structures obtained as described above, treating the solute (**3**) at the UB3LYP/6−311+G(d) level. In each simulation, a harmonic potential with a large force constant (5000 mol^{-1} $Å^{-2}$) is applied, and the center of the potential is moved from 1.27 to 4.0 Å at a 0.5 Å/ps or 5460 MD steps of 1.0 fs.

Table 1. Bond Distances and Free Energies Obtained from Multiple Steered Molecular Dynamics (MSMD) UB3LYP/6-311+G(d) for the Cleavage of the N−N Bond[a]

species	pulling direction	N−N distance (Å)	ΔG (kcal/mol)
reactant	forward	1.332	0.0
	reverse	1.343	0.0
	average	1.338	0.0
	Dutton et al.[1]	1.311	0.0
transition state	forward	1.676	4.77
	reverse	1.696	4.86
	average	1.686	4.81
	Dutton et al.[1]	1.768	7.8
products	forward	4.0	−3.78

[a] The maximum standard deviation is 2.94 kcal/mol for the reaction and 1.3 kcal/mol at the transition state.

Reverse Reaction. From the 20 final structures obtained in the pulling from reactants to products, one structure was chosen. The system is then restrained at the final distance (4.0 Å) and re-equilibrated for 3 ns using SCC-DFTB for the solute from which 20 new structures were extracted from the final 2 ns to generate an equilibrated ensemble at the final N−N separation. These 20 structures were again thermalized using the full DFT method for 1000 steps (2 ps) and then pulled in the direction of the reverse reaction, i.e., to reform the N−N bond, following the same procedure as described above.

Radial Distribution Functions. The N−N distances of 1.34 Å, 1.69 Å, and 4.00 Å were chosen as representatives of the reactants, transition state, and products (see Table 1). For those geometries, better statistics were obtained by choosing one snapshot at the desired N−N distance from each of the ten runs described for the forward reaction, and this was used as the starting configuration for a 10 ps MD run with the solute treated at the UB3LYP/6−311+G(d) level, with the N−N distance restrained to the respective value by a force constant of 5000 kcal mol^{-1} $Å^{-2}$. After the runs, the various trajectory files corresponding to each distance were combined to yield a total of 100 ps MD trajectory for the calculation of the Radial Distribution Functions (RDFs), averaged geometries, and atomic Mullkien charges.

Results and Discussion

As detailed in the previous section, the equilibrium N−N distance at the SCC-DFTB/TIP3P level was determined during equilibration to be around 1.29 Å. In order to obtain a clear minimum in Free Energy, the pulling started at a slightly smaller distance (1.27 Å) and was stopped at an N−N distance of 4.0 Å. The set of 20 pulling realizations yielded the distribution of work values shown in Figure 1 (**a**: forward, **b**: reverse reaction.) The work is set to zero at the initial simulation distance. There is a large spread in work values toward the end of the process, which is due to the finite pulling speed: at the limit of infinitely small pulling

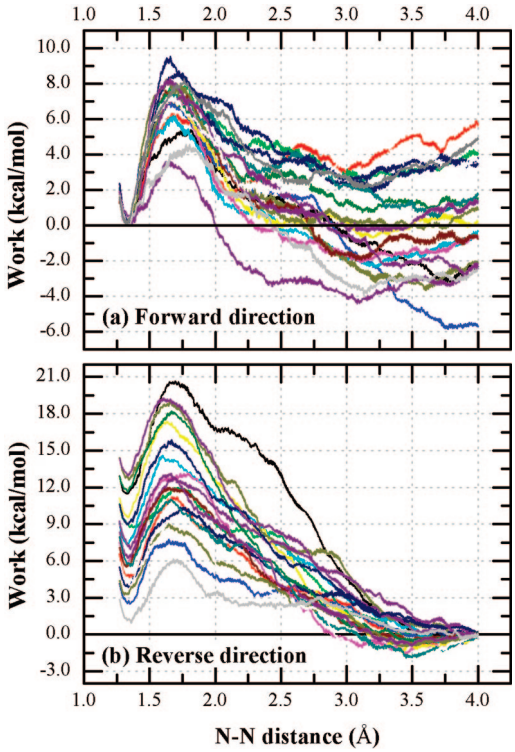

Figure 1. Work values (kcal/mol) obtained from the various realizations of the forward (a) and reverse (b) processes. The position of the zero was chosen as the reactants minimum in (a) and the products in (b).

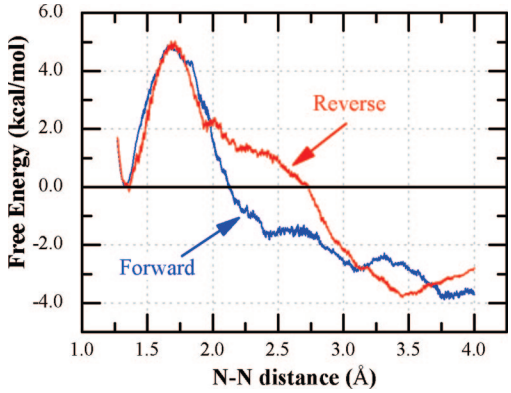

Figure 2. Free energy changes (in kcal/mol) for the breaking of the N−N bond (forward process, blue) and forming the N−N bond (reverse process, red), obtained with the Angeli's salt treated at the UB3LYP/6−311+G(d) level. Each curve is the average of 20 process realizations according to eq 6.

speeds all work curves should be congruent. The maximum standard deviation occurs close to the end points of the simulations, being around 2.94 kcal/mol for the reaction (∼4.9*RT*) and just ∼1.3 kcal/mol (∼2.18*RT*) at the transition state.

The work values were averaged according to eq 6 to yield the Free Energy change as a function of N−N distance depicted in Figure 2. The free energy profiles for the forward and reverse reactions agree extremely well for N−N distances from 1.23 Å to around 1.8 Å, yielding basically the same geometries for transition state and reactant and the same activation energy. At larger distances some hysteresis can be noted between the forward and backward pulling

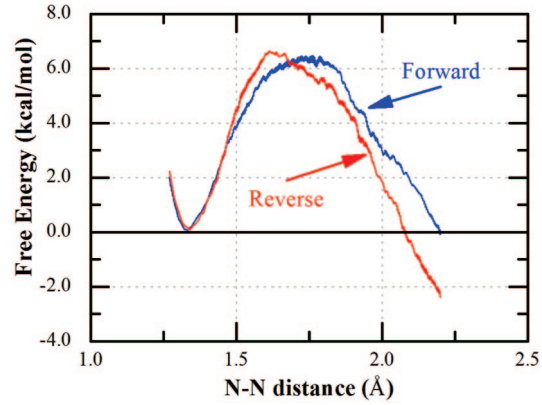

Figure 3. Free energy changes(in kcal/mol) for the breaking of the N−N bond(forward process, blue) and forming the N−N bond(reverse process, red), obtained with the Angeli's salt treated at the UMP2/6−311+G(d) level. Each curve is the average of 10 process realizations according to eq 6.

curves which can be attributed to a high pulling velocity for a charged system in an explicit water study, where the water molecules need larger relaxation times to adjust to the changing AS geometries, especially when the N−N bond is almost broken.[86] However, the free energy at the final pulling distance (∼4.0 Å) is essentially the same. The energetic data are shown in Table 1, together with results from previous calculations by Dutton et al.[1] using PCM (implicit) solvation. The distances extracted from the multiple steered molecular dynamics (MSMD) calculations are very close to the ones obtained from implicit solvation. The interaction with explicit water molecules slightly weakens the N−N bond as compared to the PCM solvation, as indicated by the facts that the N−N distance at the reactant is slightly larger (+0.03 Å) and that the transition state is reached at a smaller N−N separation (−0.1 Å) in the explicit solvent case. The difference in energies is more notable, and the presence of the explicit solvent molecules stabilizes the transition state by ∼3 kcal/mol (about 38%) compared to the PCM results. (It is important to notice that the referred PCM results include zero point energy and thermal corrections to 298 K which lower the reaction barrier by 1.80 kcal/mol. Such corrections are not explicitly included in our calculations. One can argue that while an MD derived potential of mean force includes at least part of the thermal component to the free energy, it is clear that this does not include quantized vibrations.)

Those calculations were also repeated using second order Møller−Plesset perturbation theory (MP2)[87] for the quantum region but with only 10 realizations of the process in each direction (Figure 3). The results indicate a slightly larger barrier than predicted with UB3LYP (∼6.5 kcal/mol) but still lower than the PCM results. Previous studies have shown that B3LYP generally underestimates reaction barriers by about 4 kcal/mol, while MP2 calculations can *over*estimate the same barrier by up to 6 kcal/mol.[88−90] To the best of our knowledge, there is no experimental barrier height estimate for this particular reaction. Although these barrier height errors can in principle be reduced by the use of a larger basis set, one of the previous studies has shown that, already with the 6−31+(G) basis set, the B3LYP functional can provide results with accuracy similar to the one obtained with the aug-cc-pVTZ basis set,[89] which

Table 2. Bond Distances in Å and Angles in Degrees (± Standard Deviation) for the Different Species from AS Dissociation[a]

	reactant			transition state			products	
coordinate	This work	(a)	(b)	This work	(a)	(b)	This work	(c)
O1−N1	1.252 ± 0.026	1.247	1.260	1.227 ± 0.026	1.223	1.223	1.260 ± 0.029	1.265
O3−N1	1.282 ± 0.029	1.278	1.280	1.234 ± 0.026	1.244	1.233	1.260 ± 0.029	1.265
N1−N2	1.338 ± 0.010	1.344	1.311	1.686 ± 0.009	1.637	1.768	4.000 ± 0.008	-
O2−N2	1.312 ± 0.031	1.299	1.303	1.294 ± 0.032	1.283	1.279	1.209 ± 0.019	1.200
H1−N2	1.023 ± 0.026	1.022	1.032	1.043 ± 0.029	1.042	1.049	1.060 ± 0.030	1.066
O1−N1−O3	123.9 ± 2.8	124.9	123.3	124.5 ± 3.1	124.6	123.9	116.2 ± 2.6	116.0
O1−N1−N2	119.5 ± 3.0	119.5	119.5	117.1 ± 3.9	117.9	117.1	-	-
O2−N2−N1	124.3 ± 3.6	126.0	124.3	113.6 ± 4.0	115.7	111.6	-	-
O2−N2−H1	120.8 ± 4.3	123.0	122.0	111.2 ± 3.8	112.9	110.8	109.3 ± 3.3	108.6
O1N1N2O2	−0.2 ± 13.2	12.1	−0.2	17.2 ± 14.7	25.2	17.0	-	-
O1N1N2H1	180.4 ± 14.4	171.2	179.9	132.2 ± 17.7	143.0	130.1	-	-
O1N1N2O3	−179.9 ± 7.3	−176.1	−180.0	−166.8 ± 8.6	−164.7	−165.2	-	-

[a] This work: average values and standard deviation from 100 ps MD trajectory using PUPIL/Amber, with the N−N distance restrained to the value shown. Columns marked with (a), (b), or (c) were obtained from the B3LYP/6-311+G(d) optimized structures reported in the supplemental information from Dutton et al.:[1] (a) structures optimized in vacuum; (b) structures optimized in PCM water; and (c) from the nitrite and nitroxyl structures optimized in vacuum.

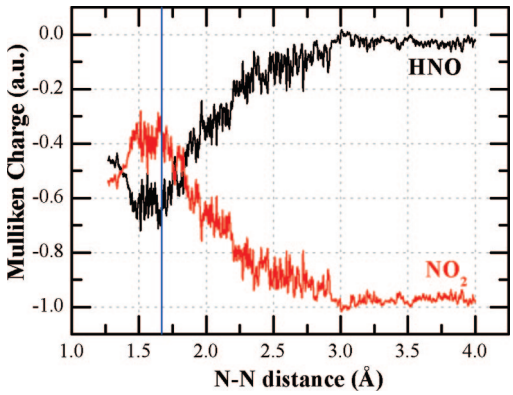

Figure 4. Average charges on the HNO and NO_2 fragments.

indicates that any error in the current calculations is more likely to be intrinsic to the B3LYP method instead of arising from basis set incompleteness issues.

To gain more insight on the nature of the species involved, additional molecular dynamics calculations were performed with the N−N distance restrained to 1.34 Å, 1.69 Å, and 4.00 Å, corresponding respectively to reactant, transition state, and product, and Table 2 compares the geometrical properties of the different species. The values obtained by Dutton et al.[1] are also included as a reference. In general, the values obtained in this work agree well with previous calculations. In most cases, the reoptimization of the vacuum structures in PCM generally brings the distances closer to the ones obtained in explicit water.[1] The largest discrepancies are noted in the N−N distances: the distance for the reactant in explicit water is very similar to the result obtained in vacuum (Δd=0.006 Å) and addition of PCM considerably shortens this distance (Δd=−0.027 Å), while the opposite effect is seen at the transition state where Δd=−0.049 Å is obtained from gas phase calculation and a larger difference (Δd=0.082 Å) under PCM calculations.

Figure 4 shows the Mulliken charge in each fragment (NO_2 in red and HNO in black) as a function of reaction coordinate, averaged from all the forward pullings using eq 8. The blue vertical line marks the N−N distance at the transition state (∼1.67 Å, as determined from the forward reaction). The averaged Mulliken charges for the 100 ps MD trajectory over each atom and moiety are shown in Table 3.

Table 3. Mulliken Charges and Standard Deviation for Different Species from AS Dissociation, Obtained from 100 ps MD Trajectory Using PUPIL/Amber[a]

atom	reactant	transition state	products
O1	−0.27 ± 0.07	−0.19 ± 0.06	−0.33 ± 0.07
N1	0.12 ± 0.08	−0.02 ± 0.00	−0.30 ± 0.07
O3	−0.37 ± 0.07	−0.20 ± 0.06	−0.34 ± 0.07
total	−0.52	−0.41	−0.97
O2	−0.48 ± 0.06	−0.43 ± 0.07	−0.07 ± 0.04
N2	−0.41 ± 0.07	−0.49 ± 0.07	−0.33 ± 0.04
H1	0.41 ± 0.07	0.34 ± 0.04	0.38 ± 0.04
total	−0.48	−0.58	−0.02

[a] The N−N distance has been restrained to 1.338, 1.686, and 4.000 Å for reactant, TS, and products, respectively.

At the N−N equilibrium distance the charge for each moiety is about the same (∼−0.5 au). As the N−N distance increases there's initially a slight polarization in the HNO direction, due to a charge transfer mainly from the NO_2 oxygens to the nitrogens involved in the N−N bond, as seen by the decrease in the (negative) charge from the oxygens and corresponding increase on the nitrogens. After the transition state most of the excess charge in the HNO moiety is transferred to the NO_2 side, and after ∼3 Å the charges at each fragment are stabilized and the bond can be considered broken.

Figure 5 shows the radial distribution functions of water molecules around the solute for the reactant, transition state, and products. It is important to notice that, at an N−N distance of 4.0 Å, the two fragments are still interacting and the HNO hydrogen (H1) tends to form a hydrogen bond to the NO_2 oxygens as shown in Figure 6, in detriment of the H-bond between it and water molecules, which explains the absence of a H-bond structure around H1 in the products (Figure 5a). The H-bond structure also disappears around the HNO oxygen (O2, Figure 5b), due to its reduced charge in the product (Table 3). Since the transition state structure is close to the reactants, one would expect the reactants and TS RDFs

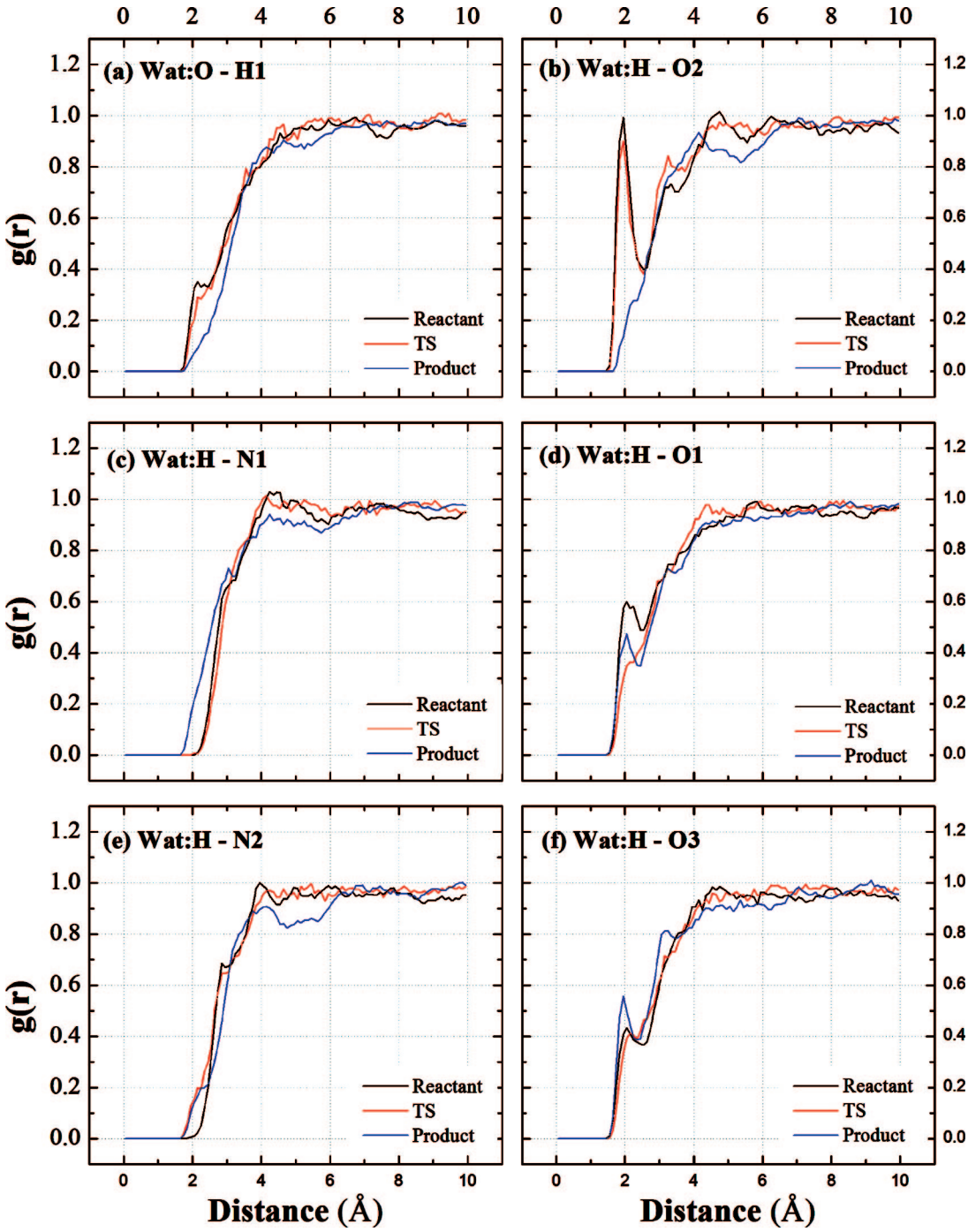

Figure 5. Radial distribution function (RDF) between water and Angeli's salt atoms (AS) for reactants, transition state (TS), and products (HNO,NO_2^-).

to be mostly similar, and this is clearly what happens in most cases. The small change in the RDFs from the reactants to transition states is mainly due to the reduction of charge in those atoms. The most noticeable difference is in Figure 5d. As seen in Table 3, the charge on O1 greatly decreases going from reactants to TS which, together with the fact that the charge in O2 is mostly constant in the same range, explains the absence of the clear H-bond around O1 in the TS. The charge in O1 is then restored in the products, and a new H-bond is formed as shown. A similar hydrogen bond also seems to form with O3 in the product (Figure 5f). Charges over the N1 atom (see Table 3) from NO_2^- product are more negative ($q_{N1}=-0.30$ au) than in the reactant ($q_{N1}=0.12$ au) and from the transition state ($q_{N1}=-0.02$ au). That can easily induce a closer distance between water hydrogen and the N1 atom as it is shown in Figure 5c. The effect of the (negative) charge increase in N2 going from reactant to TS can be noted in Figure 5e, with the water molecules at a slightly shorter distance in the TS.

Conclusions

We have presented a QM/MM study of the Angeli's salt dissociation in explicit water using the recently developed Gaussian/PUPIL/Amber interface, where the Angeli's salt

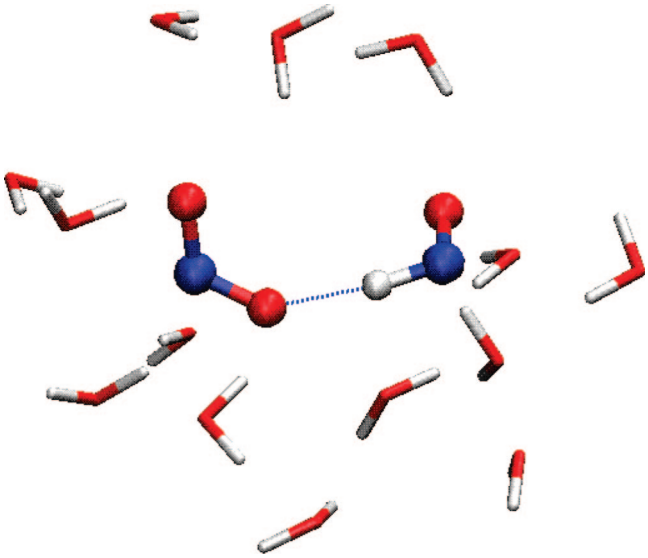

Figure 6. Representative snapshot of the products forming an internal hydrogen bond, extracted from the 100 ps trajectory with the N−N distance restrained to 4.0 Å. For clarity, only the water molecules within 3.5 Å of the solute are shown.

is treated by quantum mechanics at the UB3LYP/6−311+G(d) level and the environment (water and counterion) are treated classically. The multiple steered molecular Dynamics (MSMD) was applied together with the Jarzinsky relationship to determine the free energy change for the reaction. A free energy barrier of 4.81 kcal mol^{-1} is obtained, ∼3 kcal mol^{-1} lower than previously reported by Dutton et al.[1] using an implicit (PCM) representation for the solvent effects, at the same level of quantum calculation. Preliminary calculations using MP2 and the same basis set for the quantum zone show a higher barrier (∼6.5 kcal/mol) but still lower than the previously reported values. The geometries, averaged over the QM/MD trajectory, in general agree with the values reported by Dutton et al.[1]

Acknowledgment. This material is based upon work also supported by the NSF under the following programs: Partnerships for Advanced computational Infrastructure, Distributed Terascale Facility (DFT) and Terascale Extensions: Enhancements to the Extensible Terascale Facility. The authors thank the University of Florida High-Performance Computing Center and Teragrid (Grants TG-MCA05S010 and TG-CHE060072T) for providing computational resources and support. This work was partially funded by grant CHE-0822935 to A.E.R.

References

(1) Dutton, A. S.; Fukuto, J. M.; Houk, K. N. *J. Am. Chem. Soc.* **2004**, *126*, 3795–3800.

(2) Torras, J.; Seabra, G. d. M.; Deumens, E.; Trickey, S. B.; Roitberg, A. E. *J. Comput. Chem.* **2008**, *29*, 1564–1573.

(3) Angeli, A. *Gazz. Chim. Ital.* **1896**, *26*, 17.

(4) Angeli, A. *Gazz. Chim. Ital.* **1903**, *33*, 245–252.

(5) Fitzhugh, A. L.; Keefer, L. K. *Free Radical Biol. Med.* **2000**, *28*, 1463–1469.

(6) Naughton, P.; Foresti, R.; Bains, S. K.; Hoque, M.; Green, C. J.; Motterlini, R. *J. Biol. Chem.* **2002**, *277*, 40666–40674.

(7) Miranda, K. M.; Dutton, A. S.; Ridnour, L. A.; Foreman, C. A.; Ford, E.; Paolocci, N.; Katori, T.; Tocchetti, C. G.; Mancardi, D.; Thomas, D. D.; Espey, M. G.; Houk, K. N.; Fukuto, J. M.; Wink, D. A. *J. Am. Chem. Soc.* **2005**, *127*, 722–731.

(8) Wink, D. A.; Miranda, K. M.; Katori, T.; Mancardi, D.; Thomas, D. D.; Ridnour, L.; Espey, M. G.; Feelisch, M.; Colton, C. A.; Fukuto, J. M.; Pagliaro, P.; Kass, D. A.; Paolocci, N. *Am. J. Physiol. Heart Circ. Physiol.* **2003**, *285*, H2264–2276.

(9) Mierts, S.; Scrocco, E.; Tomasi, J. *J. Chem. Phys.* **1981**, *55*, 117–129.

(10) Tomasi, J.; Persico, M. *Chem. Rev.* **1994**, *94*, 2027–2094.

(11) RCammi, J. T. *J. Comput. Chem.* **1995**, *16*, 1449–1458.

(12) Cossi, M.; Barone, V.; Cammi, R.; Tomasi, J. *Chem. Phys. Lett.* **1996**, *255*, 327–335.

(13) McQuarrie, D. A. *Statistical Thermodynamics*; Harper and Row: New York, 1973.

(14) Kelly, C. P.; Cramer, C. J.; Truhlar, D. G. *J. Phys. Chem. A* **2006**, *110*, 2493–2499.

(15) Kongsted, J.; Mennucci, B. *J. Phys. Chem. A* **2007**, *111*, 9890–9900.

(16) Roitberg, A. E.; Worthington, S. E.; Holden, M. J.; Mayhew, M. P.; Krauss, M. *J. Am. Chem. Soc.* **2000**, *122*, 7312–7316.

(17) Worthington, S. E.; Roitberg, A. E.; Krauss, M. *J. Phys. Chem. B* **2001**, *105*, 7087–7095.

(18) Guedes, R. C.; Coutinho, K.; Costa Cabral, B. J.; Canuto, S. *J. Phys. Chem. B* **2003**, *107*, 4304–4310.

(19) Rocha, W. R.; Martins, V. M.; Coutinho, K.; Canuto, S. *Theor. Chem. Acc.* **2002**, *108*, 31–37.

(20) Rocha, W. R.; Coutinho, K.; de Almeida, W. B.; Canuto, S. *Chem. Phys. Lett.* **2001**, *335*, 127–133.

(21) Coutinho, K.; Saavedra, N.; Serrano, A.; Canuto, S. *THEOCHEM* **2001**, *539*, 171–179.

(22) Rocha, W. R.; De Almeida, K. J.; Coutinho, K.; Canuto, S. *Chem. Phys. Lett.* **2001**, *345*, 171–178.

(23) Field, M. J.; Bash, P. A.; Karplus, M. *J. Comput. Chem.* **1990**, *11*, 700–733.

(24) Warshel, A.; Levitt, M. *J. Mol. Biol.* **1976**, *103*, 227–249.

(25) Gao, J.; Xia, X. *Science* **1992**, *258*, 631–635.

(26) Gao, J. *J. Phys. Chem.* **1992**, *96*, 537–540.

(27) Case, D. A.; Darden, T. A.; Cheatham, T. E., III; Simmerling, C. L.; Wang, J.; Duke, R. E.; Luo, R.; Crowley, M.; Walker, R. C.; Zhang, W.; Merz, K. M.; Wang, B.; Hayik, S.; Roitberg, A.; Seabra, G.; Kolossváry, I.; Wong, K. F.; Paesani, F.; Vanicek, J.; Wu, X.; Brozell, S. R.; Steinbrecher, T.; Gohlke, H.; Yang, L.; Tan, C.; Mongan, J.; Hornak, V.; Cui, G.; Mathews, D. H.; Seetin, M. G.; Sagui, C.; Babin, V.; Kollman, P. A. *AMBER 10*; University of California: San Francisco, 2008.

(28) Seabra, G. M.; Walker, R. C.; Elstner, M.; Case, D. A.; Roitberg, A. E. *J. Phys. Chem. B* **2007**, *111*, 5655–5664.

(29) Walker, R. C.; Crowley, M. F.; Case, D. A. *J. Comput. Chem.* **2008**, *29*, 1019–1031.

(30) Car, R.; Parrinello, M. *Phys. Rev. Lett.* **1985**, *55*, 2471.

(31) Schlegel, H. B.; Millam, J. M.; Iyengar, S. S.; Voth, G. A.; Daniels, A. D.; Scuseria, G. E.; Frisch, M. J. *J. Chem. Phys.* **2001**, *114*, 9758–9763.

(32) Pulay, P.; Fogarasi, G. *Chem. Phys. Lett.* **2004**, *386*, 272–278.

(33) Sherwood, P.; de Vries, A. H.; Guest, M. F.; Schreckenbach, G.; Catlow, C. R. A.; French, S. A.; Sokol, A. A.; Bromley, S. T.; Thiel, W.; Turner, A. J.; Billeter, S.; Terstegen, F.; Thiel, S.; Kendrick, J.; Rogers, S. C.; Casci, J.; Watson, M.; King, F.; Karlsen, E.; Sjovoll, M.; Fahmi, A.; Schafer, A.; Lennartz, C. *THEOCHEM* **2003**, *632*, 1–28.

(34) Harvey, J. N. *Faraday Discuss.* **2004**, *127*, 165–177.

(35) Torras, J.; Deumens, E.; Trickey, S. B.; Cheng, H.-P.; Cao, C.; He, Y.; Muralidharana, K.;Roitberg, A. E.; Seabra, G. M. *University of Florida Quantum Theory Project*; 2008.

(36) Torras, J.; Deumens, E.; Trickey, S. B. *J. Comput.-Aided Mater. Des.* **2006**, *13*, 201–212.

(37) Torras, J.; He, Y.; Cao, C.; Muralidharana, K.; Deumens, E.; Cheng, H.-P.; Trickey, S. B. *Comput. Phys. Commun.* **2007**, *177*, 265–279.

(38) Frisch, M. J.; Trucks, G. W.; Schlegel, H. B.; Scuseria, G. E.; Robb, M. A.; Cheeseman, J. R. Montgomery, J. A., Jr.; Vreven, T.; Kudin, K. N.; Burant, J. C.; Millam, J. M.; Iyengar, S. S.; Tomasi, J.; Barone, V.; Mennucci, B.; Cossi, M.; Scalmani, G.; Rega, N.; Petersson, G. A.;Nakatsuji, H.; Hada, M.; Ehara, M.; Toyota, K.; Fukuda, R.; Hasegawa, J.; Ishida, M.; Nakajima, T.; Honda, Y.; Kitao, O.; Nakai, H.; Klene, M.; Li, X.; Knox, J. E.; Hratchian, H. P.;Cross, J. B.; Bakken, V.; Adamo, C.; Jaramillo, J.; Gomperts, R.; Stratmann, R. E.; Yazyev, O.;Austin, A. J.; Cammi, R.; Pomelli, C.; Ochterski, J. W.; Ayala, P. Y.; Morokuma, K.; Voth, G. A.; Salvador, P.; Dannenberg, J. J.; Zakrzewski, V. G.; Dapprich, S.; Daniels, A. D.; Strain, M. C.; Farkas, O.; Malick, D. K.; Rabuck, A. D.; Raghavachari, K.; Foresman, J. B.; Ortiz, J. V.; Cui, Q.; Baboul, A. G.; Clifford, S.; Cioslowski, J.; Stefanov, B. B.; Liu, G.; Liashenko, A.; Piskorz, P.; Komaromi, I.; Martin, R. L.; Fox, D. J.; Keith, T.; Al-Laham, M. A.; Peng, C. Y.;Nanayakkara, A.; Challacombe, M.; Gill, P. M. W.; Johnson, B.; Chen, W.; Wong, M. W.;Gonzalez, C.; Pople, J. A. Gaussian, Inc.: Wallingford, CT,2004.

(39) Case, D. A.; Cheatham, T. E., III; Darden, T.; Gohlke, H.; Luo, R.; Merz, K. M., Jr.; Onufriev, A.; Simmerling, C.; Wang, B.; Woods, R. J. *J. Comput. Chem.* **2005**, *26*, 1668–1688.

(40) Jorgensen, W. L. *J. Am. Chem. Soc.* **1981**, *103*, 335–340.

(41) Xiong, H.; Crespo, A.; Marti, M.; Estrin, D.; Roitberg, A. *Theor. Chem. Acc.* **2006**, *116*, 338–346.

(42) Jarzynski, C. *Phys. Rev. Lett.* **1997**, *78*, 2690–2693.

(43) Riccardi, D.; Li, G.; Cui, Q. *J. Phys. Chem. B* **2004**, *108*, 6467–6478.

(44) Senn, H. M. ; Thiel, W. In *Atomistic Approaches in Modern Biology*; M. R., Ed.; Springer: Berlin, 2007; Vol. *268*, pp 173−290.

(45) Truhlar, D. G.; Gao, J.; Alhambra, C.; Garcia-Viloca, M.; Corchado, J.; Sanchez, M. L.; Villa, J. *Acc. Chem. Res.* **2002**, *35*, 341–349.

(46) Gao, J.; Truhlar, D. G. *Annu. Rev. Phys. Chem.* **2002**, *53*, 467–505.

(47) Hu, H.; Lu, Z.; Yang, W. *J. Chem. Theory Comput.* **2007**, *3*, 390–406.

(48) Major, D. T.; Gao, J. *J. Chem. Theory Comput.* **2007**, *3*, 949–960.

(49) Gunaydin, H.; Acevedo, O.; Jorgensen, W. L.; Houk, K. N. *J. Chem. Theory Comput.* **2007**, *3*, 1028–1035.

(50) Bowman, A. L.; Ridder, L.; Rietjens, I. M. C. M.; Vervoort, J.; Mulholland, A. J. *Biochemistry (Moscow)* **2007**, *46*, 6353–6363.

(51) Valiev, M.; Garrett, B. C.; Tsai, M.-K.; Kowalski, K.; Kathmann, S. M.; Schenter, G. K.; Dupuis, M. *J. Chem. Phys.* **2007**, *127*, 051102-–4.

(52) Rosta, E.; Klahn, M.; Warshel, A. *J. Phys. Chem. B* **2006**, *110*, 2934–2941.

(53) Christen, M.; Kunz, A.-P. E.; van Gunsteren, W. F. *J. Phys. Chem. B* **2006**, *110*, 8488–8498.

(54) Marsili, S.; Barducci, A.; Chelli, R.; Procacci, P.; Schettino, V. *J. Phys. Chem. B* **2006**, *110*, 14011–14013.

(55) Riccardi, D.; Schaefer, P.; Yang, Y.; Yu, H.; Ghosh, N.; Prat-Resina, X.; Konig, P.; Li, G.; Xu, D.; Guo, H.; Elstner, M.; Cui, Q. *J. Phys. Chem. B* **2006**, *110*, 6458–6469.

(56) Wales, D. J.; Bogdan, T. V. *J. Phys. Chem. B* **2006**, *110*, 20765–20776.

(57) Claeyssens, F.; Harvey, J. N.; Manby, F. R.; Mata, R. A.; Mulholland, A. J.; Ranaghan, K. E.; Schütz, M.; Thiel, S.; Thiel, W.; Werner, H.-J. *Angew. Chem., Int. Ed.* **2006**, *45*, 6856–6859.

(58) Kastner, J.; Thiel, W. *J. Chem. Phys.* **2005**, *123*, 144104–5.

(59) Roitberg, A. E. *Annu. Rep. Comp. Chem.* **2005**, *1*, 103–111.

(60) Li, G. H.; Zhang, X. D.; Cui, Q. *J. Phys. Chem. B* **2003**, *107*, 8643–8653.

(61) Park, S.; Khalili-Araghi, F.; Tajkhorshid, E.; Schulten, K. *J. Chem. Phys.* **2003**, *119*, 3559–3566.

(62) Kumar, S.; Rosenberg, J. M.; Bouzida, D.; Swendsen, R. H.; Kollman, P. A. *J. Comput. Chem.* **1995**, *16*, 1339–1350.

(63) Roux, B. *Comput. Phys. Commun.* **1995**, *91*, 275–282.

(64) Kumar, S.; Rosenberg, J. M.; Bouzida, D.; Swendsen, R. H.; Kollman, P. A. *J. Comput. Chem.* **1992**, *13*, 1011–1021.

(65) Torrie, G. M.; Valleau, J. P. *J. Comput. Phys.* **1977**, *23*, 187–199.

(66) Mulholland, A. J. *Drug Discovery Today* **2005**, *10*, 1393–1402.

(67) Warshel, A. *Computer Modeling of Chemical Reactions in Enzymes and Solution*; Wiley: New York, 1991.

(68) Woods, C. J.; Manby, F. R.; Mulholland, A. J. *J. Chem. Phys.* **2008**, *128*, 014109–8.

(69) Crooks, G. E. *Phys. Rev. E* **2000**, *61*, 2361.

(70) Hummer, G.; Szabo, A. *Proc. Natl. Acad. Sci. U.S.A.* **2001**, *98*, 3658–3661.

(71) Collin, D.; Ritort, F.; Jarzynski, C.; Smith, S. B.; Tinoco, I.; Bustamante, C. *Nature (London)* **2005**, *437*, 231–234.

(72) Cuendet, M. A. *J. Chem. Phys.* **2006**, *125*, 144109–12.

(73) Hermans, J. *J. Phys. Chem.* **1991**, *95*, 9029–9032.

(74) Elstner, M. *Theor. Chem. Acc.* **2006**, *116*, 316–325.

(75) Dixon, S. L.; Merz, J. K. M. *J. Chem. Phys.* **1996**, *104*, 6643–6649.

(76) Yang, W.; Lee, T.-S. *J. Chem. Phys.* **1995**, *103*, 5674–5678.

(77) Dixon, S. L.; Merz, J. K. M. *J. Chem. Phys.* **1997**, *107*, 879–893.

(78) Wang, J.; Wolf, R. M.; Caldwell, J. W.; Kollman, P. A.; Case, D. A. *J. Comput. Chem.* **2004**, *25*, 1157–1174.

(79) Jakalian, A.; Bush, B. L.; Jack, D. B.; Bayly, C. I. *J. Comput. Chem.* **2000**, *21*, 132–146.

(80) Jakalian, A.; Jack, D. B.; Bayly, C. I. *J. Comput. Chem.* **2002**, *23*, 1623–1641.

(81) Ryckaert, J.-P.; Ciccotti, G.; Berendsen, H. J. C. *J. Comput. Phys.* **1977**, *23*, 327–341.

(82) Otte, N.; Scholten, M.; Thiel, W. *J. Phys. Chem. A* **2007**, *111*, 5751–5755.

(83) Becke, A. D. *J. Chem. Phys.* **1993**, *98*, 5648–5652.

(84) Frisch, M. J.; Pople, J. A.; Binkley, J. S. *J. Chem. Phys.* **1984**, *80*, 3265–3269.

(85) Krishnan, R.; Binkley, J. S.; Seeger, R.; Pople, J. A. *J. Chem. Phys.* **1980**, *72*, 650–654.

(86) GonzalezLebrero, M. C.; Estrin, D. A. *J. Chem. Theory Comput.* **2007**, *3*, 1405–1411.

(87) Møller, C.; Plesset, M. S. *Phys. Rev.* **1934**, *46*, 618.

(88) Zhao, Y.; Gonzalez-Garcia, N.; Truhlar, D. G. *J. Phys. Chem. A* **2005**, *109*, 2012–2018.

(89) Riley, K. E.; Op'tHolt, B. T.; Merz, K. M. *J. Chem. Theory Comput.* **2007**, *3*, 407–433.

(90) Sousa, S. F.; Fernandes, P. A.; Ramos, M. J. *J. Phys. Chem. A* **2007**, *111*, 10439–10452.

CT800236D